Prepared for submission to JCAP

Model-Independent Cosmological Tests

Michael Scott Peck[a]

[a]Independent

E-mail: theonestation@hotmail.com

Abstract. Several non-fiducial cosmological tests are discussed allowing various models to be conclusively differentiated from one another. The four models tested include ΛCDM, the Friedmann-Lemaître metric and a recently proposed steady state with and without local expansion. The cosmological tests range from redshift versus distance modulus to the angular size and time dependence of distant objects. Recent observations allow strict constraints on both the size and evolution of faint blue galaxies up to 23B. The solution to the faint blue galaxy problem is further discussed relative to size versus absolute magnitude, number densities and observations of minimal evolution. Models with expanding metrics are ruled out due to incorrect predictions of angular diameter distance and time-dependence. Observations instead depict a steady state universe with asymptotically flat gravitational potential and embedded bulk flows.

Keywords: Cosmology, Faint Blue Galaxies, Galaxy Formation, Galaxy Evolution, Galaxy Clusters

Submitted October 9th, 2013

1 Introduction

Direct observations over 30 years now allow several model-independent cosmological tests to be conducted. These tests can easily differentiate between models, providing conclusive results on their validity. The dynamics and curvature of the universe are determined by several cosmological parameters, providing redshift versus luminosity distance and angular diameter distances. The first can be confirmed with SNIa due to their nearly uniform properties, i.e. they are standard candles. The later requires various direct observations of galaxies, clusters and number densities. Recent observations have allowed strict constraints on mergers, luminosity evolution and the amount of common disk galaxies up to moderate redshift. Faint blue galaxies (FBGs) are therefore superior in terms of measuring angular diameter distances and number densities.

The faint blue galaxy problem is known as a grand cosmological issue for several reasons (He et al. 1998) [18]. A $2x$ excess of FBGs with respect to no-evolution ΛCDM is observed up to 22.5B (Colless et al. 1989) [6], increasing to $3x$ by 24.0B (Driver et al. 1996) [10]. At least half of the 2x excess is observed to occur prior to $0.5z$ with respect to spectroscopic surveys (Colless et al. 1989) [6]; the $3x$ excess occurs prior to $1.0z$ (Roche et al. 1997) [40]. These were found to be consistent with various types of common disks (Colless et al. 1994) [7]. The redshift versus distance modulus and properties of FBGs were also consistent with minimal evolution for 22.5B (Colless et al. 1989) [6]. This problem is demonstrated to arise from the assumption of $D_L = D_A(1+z)^2$.

By measuring the major axis diameters of FBGs with respect to surface brightness limits, each can be compared to local populations. It is observed that the size versus absolute B-band magnitudes of these galaxies is fit by a static space-time metric with slightly negative curvature. This is confirmed by measuring the angular diameters of the largest clusters up to extreme redshift. Applying the largest objects at various redshift allows any uncertainty due to morphological evolution to be ignored. Galaxies and clusters are demonstrated to have nearly equivalent variations in angular diameters with respect to redshift. Combined with observations of minimal evolution and the 2 - 3x abundance of FBGs, models that generate cosmological redshift from metric expansion are ruled out. The steady state however is found to be in agreement with the angular size, redshift distribution and number densities of FBGs.

The time dependence of the various models is further tested by knowing the amount of mergers experienced by 1.35z (Lotz et al. 2011) [29], merger fractions (Kartaltepe et al. 2007) [22] and merger times from simulations (Lotz et al. 2008) [28]. These results are applied to determine expected number densities of FBGs with minimal evolution over 20B to 23B. Various observations are discussed relative to proper age increasing with redshift. These include the lack of local merger remnants, increasing cold baryonic matter with redshift and relatively higher metallicity for distant objects. Morphological evolution is then discussed for common galaxies including star formation and significance of x-ray emitting gas.

2 Methods

The models compared include ΛCDM, the Friedmann-Lemaître metric and steady state with and without residual thermal expansion (Peck 2013) [39]. The Big Bang theory was proposed by Lemaître (1927) [26] and Hubble (1929) [19], with the Hubble constant being the only parameter at $H_0 = 68.7\ (km \cdot s^{-1})/Mpc$. This model fails to agree with observations beyond 0.1z, requiring the addition of several parameters including $\Omega_c = 0.222$, $\Omega_\Lambda = 0.728$ and

$\Omega_b = 0.0456$; $H_0 = 70.4\ (km \cdot s^{-1})/Mpc$ is applied relative to recent ΛCDM predictions (Jarosik et al. 2011) [21]. The steady state requires two parameters, where the slope of an asymptotically flat potential is set to $S_0 = 3.248 \pm 0.047 \cdot 10^{42}\ (kg \cdot m \cdot s^{-2})/Gpc$ and y-intercept $y_0 = 0.375 \pm 0.161\ Gpc$ (Peck 2013) [39]. The inferred accelerated expansion is predicted to arise from the deflection of light in an asymptotically flat gravitational potential. The full range of redshift versus distance modulus is therefore obtained by varying the y-intercept from 0.0 to 0.536 Gpc for a steady state without local expansion. However, y_0 actually depicts the average distance to the start of flow into a global gravitational potential over all local directions.

The redshift equation for the steady state model is derived from relativistic Doppler and gravitational redshift. Vacuum energy density in equation (2.1) is directly related to gravitational potential by $\mathbf{\nabla} = -{c_0}^2\Phi/G_0$.

$$z = \frac{G_0}{{c_0}^4}\left(\sqrt{\mathbf{\nabla}\left(\mathbf{\nabla} + \frac{2{c_0}^4}{G_0}\right)} + 2\mathbf{\nabla}\right) \tag{2.1}$$

The local region ($< 0.1z$) however is observed to have residual thermal expansion. This is well described by the Friedmann-Lemaître metric, but with D_A equivalent to D_L; i.e. the metric is static and only matter upon it is receding. Since redshift in the steady state with local expansion is predicted to originate from two sources, the Friedmann-Lemaître model is smoothed with predictions between 0.1z and 0.2z. The local expansion will therefore be the main component with respect to distance modulus versus redshift prior to $0.1z$, becoming less dominate beyond.

Vacuum energy density produces a locally isotropic metric with angular diameter distance defined by equation (2.2). Luminosity distance in this perspective is equivalent to metric distance, where vacuum energy density is defined with $\mathbf{\nabla} = \mathrm{S_0}\,(\mathrm{D_L} - \mathrm{y_0})$. Low redshift ($\mathrm{D_L} \leq \mathrm{y_0}$) is best described by $\mathrm{D_L}$=$\mathrm{D_A}$ since local variations in vacuum energy density are minimal.

$$\mathrm{D_A} \cong \mathrm{D_L}\left(1 + \frac{S_0 G_0}{{c_0}^4}\,(\mathrm{D_L} - y_0)\right) \tag{2.2}$$

For a steady state with local expansion, distance modulus is divided into three regions. Redshift prior to 0.1z is dominated by residual thermal expansion and bulk flows. For $0.1 < z < 0.2$, the acceleration with respect to the average flow into the gravitational potential (μ_Φ) is smoothed with local expansion (μ_H) via equation (2.3). k is set to $5\pi(z - 0.1)$, with remaining redshift defined by the steady state model.

$$\mu = \mu_H \cos^2(k) + \mu_\Phi \sin^2(k) \tag{2.3}$$

The first cosmological test applies SNIa data obtained from NED (2013) [35] to verify predictions of redshift versus distance modulus. SNIa are standard candles with respect to their uniform properties, making them suitable for model-independent tests. Local expansion is also tested with respect to any dispersion of SNIa data. If the local space is dominated by residual thermal expansion, there must be minimal directional dependence. If the local space lacked residual thermal expansion, a slight dipole would arise. For example, directions pointed

into the global gravitational potential have redshift increasing faster with respect to distance modulus. The opposite direction will have similar predictions, where the local space is moving at a faster rate relative to objects at a higher potential. After sufficient distance, the majority of objects with respect to Earth are projected from a lower gravitational potential. This provides the illusion of accelerated metric expansion due to the nearly spherical projection of space towards the center of an asymptotically flat gravitational potential.

The second set of tests provides additional constraints on cosmological metrics, where the angular diameters of galaxies and clusters are measured. These objects are suitable for model independent tests for several reasons. The faint blue galaxies prior to 23.0B are well constrained from numerous observations and studies. For example, it is known that the properties of these galaxies are consistent with minimal evolution; i.e. they are similar to local blue galaxies. The availability of high-resolution imaging further allows sufficient observations up to 0.7z. By measuring the major axis diameters of local blue galaxies and the more distant populations, the absolute B-band magnitudes can be compared. The local dataset contains 567 blue galaxies with maximum luminosity distance of 50 Mpc. These consist of a wide range of disk and irregular populations, including both face-on and edge-on galaxies. Morphologies consisted of 108 Scd, 84 Sc, 64 Sbc, 64 Im, 61 Sd, 31 Sdm, 28 Sm, 19 Sab, 16 Sa, five I0 and 21 unidentified spiral galaxies (NED 2013) [35]. Major axis diameters are applied to reduce the dependence on orientation. The diameters of local galaxies were obtained from Nilson (1973) [36] and de Vaucouleurs et al. (1991) [49] relative to 25.0 B mag $\cdot$ arcsec^{-2} surface brightness limits.

The FBGs require several constraints in order to demonstrate minimal evolution. The redshift distribution of these galaxies is consistent with no evolution relative to ΛCDM (Colless et al. 1989) [6] and the steady-state models. Non-fiducial studies further confirmed that the amount of mergers prior to $0.5z$ is insufficient to affect galactic evolution. For example, galaxies on average experience a single major merger by $1.35z$ (Lotz et al. 2011) [29]. Studies have ruled out any evolution at the faint end of the spectrum (Gronwall et al. 1995) [14], with minimal evolution at the bright end prior to $0.5z$ (Broadhurst et al. 1988) [4]. The high-resolution imaging of FBGs up to 23.0B provided by Colless et al. (1994) [7] also depicts common galaxies. These FBGs are listed in table **1** and have nearly identical properties to local examples. From these 24 FBGs, two were elliptical galaxies, 20 were common disk and the remaining two were dwarfs or irregular. Absolute magnitudes of these FBGs also increase with redshift, i.e. comparing major axis diameters to absolute magnitude is similar to angular size versus redshift of clusters. Equal disagreement for the angular diameter of FBGs and clusters would therefore demonstrate incorrect angular diameter distances, which varies proper volume and number densities.

Several problems arise when attempting to compare the size of local galaxies with the faint blue galaxies provided by Colless et al. (1994) [7]. The first is the diversity of morphologies, which range from high surface brightness dwarfs to a giant elliptical (cD). Intrinsic characteristics of each galaxy will therefore drastically vary from one another as observed by OII widths, $(b_j - r_F)$ color and surface brightness. However, the vast majority of FBGs are common disk and irregular galaxies. The only exceptions to this are FBGs beyond 0.5z, which have colors consistent with massive starburst galaxies. These are abundant at higher redshift due to UV properties, size and luminosity. Two additional outliers include an elliptical galaxy and previously mentioned cD. These early-type galaxies are intrinsically red as demonstrated by $(b_j - r_F)$ color and fail to meet the characteristics of FBGs; both are however included for reference.

Table 1. Properties of FBGs with major axis diameters measured to (top) 24.4V mag or (bottom) 25.0B mag per arcsec^{-2}

ID	Redshift $(z)_{spec}$	Dist. Mod. (u)[1]	$(m_B)^{[1]}$	$(m_B)^{[2]}$	Major Axis Diameter (“)	Morphology
10.2.05	0.303	40.84	-18.87	-19.2	2.748 ± 0.315	E
10.2.17	0.302	40.83	-18.83	-18.6	3.147 ± 0.382	Sb
10.2.23	0.665	43.09	-20.48	-19.7	2.002 ± 0.389	Sc pec Sy
13.2.10	0.424	41.78	-19.82	-20.8	3.561 ± 0.753	cD
13.2.13	0.430	41.82	-19.75	-20.0	3.095 ± 0.563	Scd pec
13.2.22	0.422	41.76	-19.32	-19.0	2.880 ± 0.235	Sd
13.4.12	0.120	38.66	-16.91	-16.8	3.294 ± 0.409	Sd
13.4.16	0.120	38.66	-16.69	-16.3	3.371 ± 0.273	Scd
13.4.22	0.086	37.92	-15.57	-15.1	3.003 ± 0.430	Im
13.5.06	0.112	38.50	-15.85	-15.5	1.838 ± 0.181	dIm pec
13.5.07	0.220	40.02	-18.45	-17.7	3.041 ± 0.374	Sc pec
13.5.10	0.329	41.06	-19.24	-19.1	4.199 ± 0.365	Sab
13.5.12	0.678	43.15	-21.27	-20.8	3.383 ± 0.484	Scd
13.5.14	0.255	40.39	-18.31	-18.8	3.848 ± 0.440	Sc
13.5.20	0.521	42.38	-19.83	-19.9	3.798 ± 0.635	Sa
10.2.02	0.549	42.53	-20.88	-19.4	2.805 ± 0.357	Sbc
10.2.04	0.543	42.50	-20.54	-19.1	2.812 ± 0.266	Scd
10.2.15	0.451	41.95	-20.00	-20.1	1.876 ± 0.633	Sb
10.2.20	0.188	39.66	-17.39	-17.5	2.600 ± 0.581	Sab
10.2.22	0.180	39.56	-17.20	-16.8	3.070 ± 0.638	Sc
13.2.17	0.202	39.82	-17.49	-17.4	1.969 ± 0.190	Sab
13.2.23	0.281	40.64	-18.06	-18.1	1.337 ± 0.802	Sa
13.2.26	0.598	42.78	-20.12	-18.6	1.977 ± 0.262	Sc
13.2.36	0.537	42.46	-19.46	-19.4	2.072 ± 0.397	Sd

[1]Distance modulus is derived from the best fitting model with spectroscopic redshift (steady state including local expansion)

[2]Best estimate from Colless et al. (1994) [7]

A second problem arises due to systematic errors within Colless et al. (1994) [7] relative to the B1, B2, I1 and I2 surface brightness profiles. The second set of FBGs provide $(B - I) < 0$ for all objects including early disk. This is illogical, as early-type disk commonly have colors around $(B - I) > 2.00$. An extreme example of this is FBG 13.2.26 with a redshift of 0.202z and $(B - I) < -2.00$ with respect to Colless et al. (1994). This galaxy is consistent with a bulge dominated disk, with $(b_j - r_F) = 1.42$ and OII width of 0. Correlating OII widths, color and surface profiles with the first set of FBGs indicates that surface brightness measurements were off by -2.07 B mag and -0.45 I mag per arcsec^{-2} for the second set. To account for any uncertainty from these errors, the FBGs were also digitalized and converted to high-resolution contours. Uncertainty in major axis diameter for table **1** is determined from the standard deviation between B or I diameters derived from Colless et al. (1994), major axis diameters in table **1** and average size of each FBG out to the faintest contours. Uncertainty in major axis diameters out to the 25B reference level however is likely less than some of these suggest.

The third issue relates to comparing galaxies imaged in the V-band to the 25B reference level. These bands provide similar measurements due to their proximity in wavelength, i.e. 4300A and 5420A respectively (Colless et al. 1994) [7]. There is however a slight error in major axis diameters without wavelength corrections. The difference between these bands is morphology dependent, where (B − V) surface colors are nearly flat for early-types. The outer extents of common disks however can have (B − V) colors of 0.4, where a correction of 0.6 is applied with respect to the average value. Relative to 25.0 B mag · arcsec^{-2} reference levels, the bulk of FBGs are common disk correspond to a 24.4 V mag · arcsec^{-2} limit. Applying these constraints allows the previous studies of local galaxy diameters to be compared with both sets of FBGs.

The interpretation of OII widths with respect to strong starburst and LINER/ Seyfert galaxies relates to the final problem. Recent observations by Lemaux et. al. (2010) [27] have demonstrated that large OII widths at high redshift ($0.8z - 0.9z$) do not necessarily correspond to nuclear starburst or extended disk activity. LINER type galaxies commonly consist of early-type galaxies with relatively high (B − R) color. This distinction allows high OII width, but redder galaxies to be differentiated from active star forming galaxies. Seyfert galaxies on the other hand occur almost exclusively with disk, making them difficult to differentiate from strong starburst galaxies. An important indication of an active galactic nuclei rather than extended starburst galaxies is the existence of significant bulges, high OII widths and relatively red colors ($b_j - r_F$) > 1.20. Mass and size of supermassive black holes are closely related to bulge mass (Häring et al. 2004) [16] and bulge luminosity. From high-resolution imaging, color and OII widths provided by Colless et al. (1994) [7], the FBGs could be directly compared to local galaxies of similar absolute B-magnitude, appearance and size. The only galaxy that could be easily differentiated as a Seyfert is 10.2.23, which has a significant bulge in the I-band, OII width of 75 and ($b_j - r_F$) = 1.29 color.

Clusters are applied for the second part of the angular scale test, where the amount of clusters measured was increased to 227 (Maughan et al. 2008, Williamson et al. 2011 and Mehrtens et al. 2012) [32, 34, 52]. This includes 189 of the most massive cluster, 22 smaller clusters and 16 Lyman-alpha blobs (Ivison et al. 1998; Keel et al. 1999; Steidel et al. 2000; Venemans et al. 2002; Dey et al. 2005; Nilsson et al. 2006; Greve et al. 2007; Saito et al. 2008; Smith et al. 2008; Hatch et al. 2009; Ouchi et al. 2009 and Willott et al. 2011) [9, 13, 17, 20, 25, 37, 38, 42, 43, 45, 50, 53]. X-ray contours were measured from the centers to 2−3 sigma above background rates; major and minor axes were then averaged. The extent of Lyman-alpha emission was instead applied to Lyman-alpha blobs. These measurements allow mergers to be differentiated from larger clusters. An active major merger for example will at most double in major axis diameter, while the average diameter increases by less than 50%. There are several clusters with average diameters less than one megaparsec, which were removed when all models except steady state without expansion predicted diameters below this limit. Since these models have similar predictions at low redshift, this ensures only the most massive clusters are included for all redshift.

The largest of clusters are applied for several reasons. Observations are limited to seeing only the largest objects at moderate to high redshift, which must be morphologically related to the largest objects at all redshift. The second reason is due to their relative angular diameters. FBGs_up to 23.0B ($< 0.7z$) have major axis diameters to the faintest contours of $3.00'' \pm 0.73''$, while Lyman-alpha blobs are $> 2''$ prior to $10z$. Faint red galaxies in the HUDF for example exist between $1.0z$ and $3.5z$ (Stutz et al. 2008) [46]. Many of these are disk galaxies and likely related to FBGs. However, averaging angular diameters to the

faintest contours provides $0.41'' \pm 0.09''$. These galaxies therefore have angular diameters nearly $10x$ smaller than the < 23B sample of FBGs, making surface brightness measurements implausible. Distance and time-scales involved in major cluster mergers are also greater than for galaxies, reducing overall variations in size.

The final cosmological tests relate to major mergers and number densities. The amount of mergers each galaxy experiences by $1.35z$ and close pair fractions of normal disk allow strict constraints on the time-dependence and number densities FBGs. Numerical simulations of major mergers have be conducted placing the average merger time around 2.88 billion years (Lotz et al. 2008) [28]. These however include dark matter, which is only theorized to exist with respect to ΛCDM. This can add up to four times the visual mass of galaxies (McDonald 2013) [33]. Simulated merger times would therefore be underestimated relative to other models. Although the applied merger time is fiducial in terms of ΛCDM, it allows for a sufficient comparison between the various models.

There is an important distinction between the time dependence of an expanding universe and steady state model. For ΛCDM, objects should appear younger as redshift increases with respect to an observer on Earth. The opposite is true for the steady state model, where objects appear older as redshift increases. Time-dependence for ΛCDM and the Friedmann-Lemaître metric is derived from previously provided parameters. The steady state's time-dependence is obtained from equation (2.4). Beyond testing models against the observed duration of proper time between $0z$ and $1.35z$, other characteristics of galaxies and clusters are able to differentiate between models. An expanding universe would for example have metallicity decreasing with redshift.

$$\frac{\triangle \mathrm{D_L}}{\triangle \tau} = \frac{1}{\triangle \mathrm{D_L}} \int_0^{\triangle \mathrm{D_L}} u\left(\mathrm{D_L}\right)\ d\mathrm{D_L} \tag{2.4}$$

Proper velocity for objects accelerating into the gravitational potential is defined by equation (2.5). The proper time applied for the steady state is determined by varying the y-intercept from 0.0 to 0.536 *Gpc* and taking the averaged value, i.e. local expansion is not considered in either case.

$$u\left(\mathrm{D_L}\right) = \frac{\mathrm{dD_L}}{\mathrm{d}\tau} = \frac{\mathrm{G_0}}{{\mathrm{c_0}}^3} \sqrt{\nabla \left(\nabla + \frac{2{\mathrm{c_0}}^4}{\mathrm{G_0}} \right)} \tag{2.5}$$

3 Results

Available SNIa data allows two of the four models to be ruled out. Although the steady state without local expansion fits observations when varying the y-intercept, local SNIa depict nearly isotropic expansion. Directional dependence of ΛCDM cosmological parameters however has been observed (Axelsson et al. 2013) [2], which is expected for the steady state. The Friedmann-Lemaître model is ruled out due to a poor fit beyond 0.1z. Each model's residual is further plotted relative to the steady state with local expansion in figure **1**. ΛCDM and the steady state with expansion provide similar standard deviations of 0.5381 and 0.5305 respectively. These results do not allow the models to be differentiated beyond testing for locally isotropic expansion beyond $0.1z$.

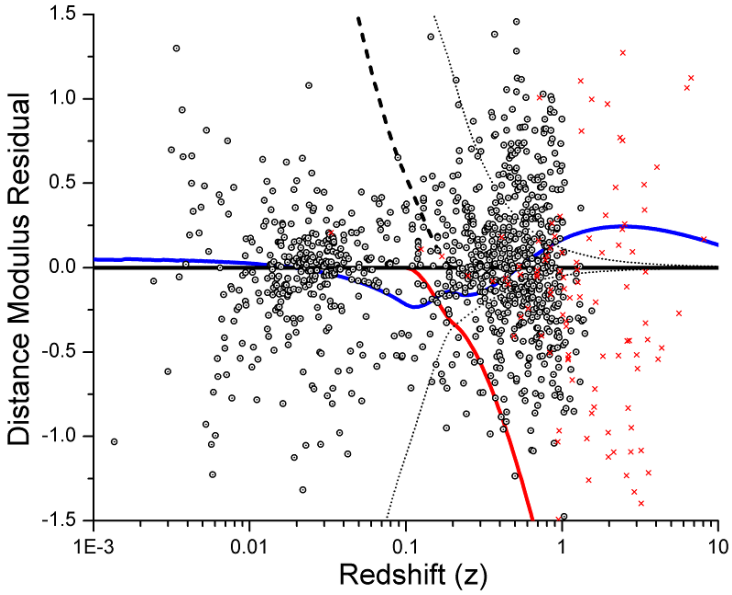

Figure 1. 1005 SNIa compared between the four models. The thick black line is the steady state with local expansion, while the dashed line is without. The thin dotted lines are the limits of the steady state model by varying the y-intercept from 0 to 0.536 Gpc. Blue is ΛCDM with the Friedmann-Lemaître in red. Red data points are GRBs (Wei 2010) [51] that were not included in the standard deviation.

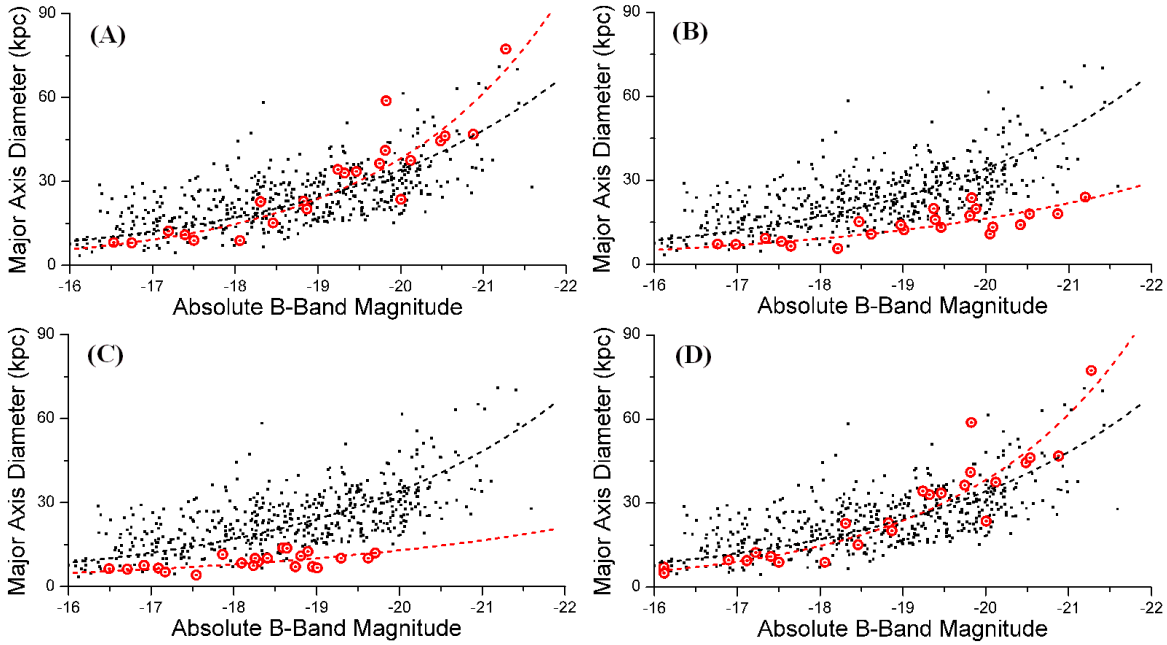

Figure 2. Size versus absolute B-band magnitudes of distant and local blue galaxies. The red line represent the FBGs logarithmic fit for (**A**) the steady state with expansion (**B**) ΛCDM (**C**) Friedmann-Lemaître metric and (**D**) steady state without local expansion. The standard deviation for local galaxies at these magnitudes is 8.490, while the models provide standard deviations of 8.836, 15.01, 11.12 and 8.840 respectively.

The angular scale tests provide conclusive results, as angular diameter distances drastically differ between models. The plots in figure **2** compare the predictions of each model with respect to the FBGs from Colless et al. (1994) [7]. With minimal evolution occurring up to these magnitudes, the imaged FBGs are expected to be identical to local blue galaxies. However, data points for ΛCDM and Friedmann-Lemaître are all below the trend for local galaxies. The steady state models are in agreement with observations except for two data points. These include a giant elliptical (cD) around -20 mB and the brightest galaxy of the survey at -21.27 mB. cD galaxies commonly have diameters ranging from 50 to 100 kpc and do not fit the properties of FBGs, i.e. they are anomalies. The large disk around -21.27 mB is in the process of undergoing a major merger, causing a slightly overestimated absolute B-magnitude. Figure **2** compares the 24 FBGs and 568 local galaxies for each model.

The FBGs are well constrained in terms of major axis diameters and evolution up to 23B. However, they are limited to moderate redshift ($< 0.7z$) relative to these magnitudes. Clusters are much larger, allowing cosmological tests to be extended to higher redshift. The major and minor axes were measured up to $2-3$ sigma above background rates and averaged to reduce the effects of active mergers. A major merger between two clusters would for example have the averaged x-ray contours increased by 50% at most. Actual uncertainty is well below 20% for the clusters applied in figure **3**. To put models on equal footing, the average diameter relative to each model between $0z$ and $0.5z$ is applied. These predictions are further extended between one and six megaparsecs.

Simulations of major cluster mergers usually require relaxation times of five billion years or more (Roettiger et al. 1999) [41]. Merger fractions for clusters are estimated to be between 0.1 and 0.5 (Mann et al. 2011) [31]. These fractions however are overestimated for angular diameter distances derived from ΛCDM, i.e. much larger separation distances are included with increased redshift. With major mergers being the main factor in the evolution of cluster sizes, this would imply that average diameters should not drastically vary beyond $0.7z$. Whether mergers play a significant role in the angular size of distant clusters, the most massive objects at any redshift must be directly related to each other. This requires the most massive clusters to be directly related to distant Lyman-alpha blobs.

All data points beyond $2z$ consist of Lyman-alpha blobs, which are the largest objects at high redshift. These distant clusters are surrounded by large amounts of reionized hydrogen rather than hot x-ray emitting gas. With respect to angular diameters of the clusters in figure **3**, models that generate redshift from expanding metrics predict for these objects to be tens to hundreds of times larger than observed. However, the steady state predicts for Lyman-alpha blobs to be identical in size to local clusters as depicted in figure **3**. These observations are consistent with minimal variations in size up to high redshift.

The geometric standard deviation is applied to determine the fit of clusters for several reasons. (**I**) Plotting the angular diameters of clusters on a log-log scale allows the various models to be easily differentiated, while the vertical width of data points and predictions are nearly equivalent for all z. This allows for the possibility of a log-normal distribution without favoring any model. (**II**) Current observations are likely skewed by an abundance of small clusters locally and large clusters at high redshift due to observational limitations. (**III**) Distant clusters are off by a factor of $100x$ with respect to ΛCDM; this equates to an error of about 1700 kpc. The steady state has a higher prediction for the angular size of clusters at low redshift, where at most the model is off by a factor of about $2x$. This in return results in an error of 1500 kpc, similar to that of the 1700 kpc for high redshift ΛCDM predictions.

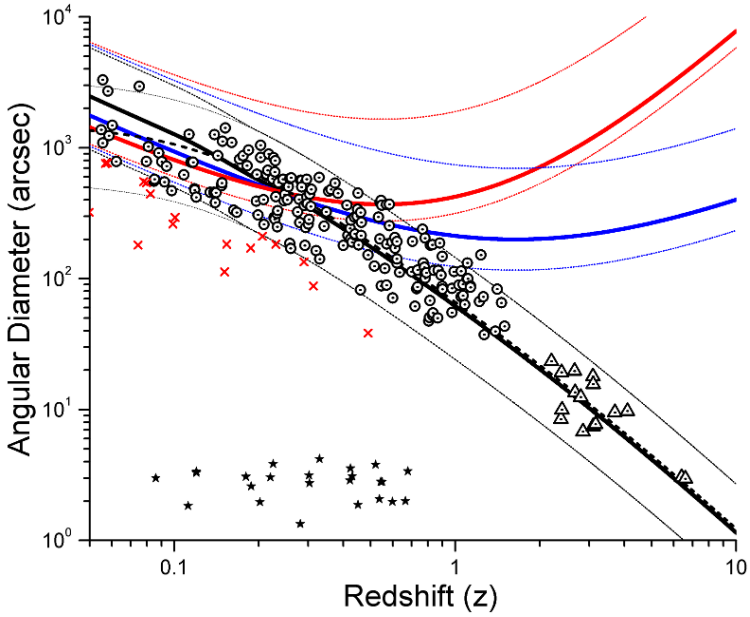

Figure 3. Angular diameters of **227** clusters compared between the four models. Triangles represent Lyman-alpha blobs, while filled stars are FBGs from figure **2**. Excluded clusters that were smaller than one megaparsec are red **x**.

The trend of massive clusters is found to be consistent with FBGs, where the steady state without local expansion is superior at 0.2054. This result is likely due to the slightly higher average diameter obtained between $0.1z$ and $0.5z$. The steady state with local expansion has a geometric standard deviation of 0.2192, while ΛCDM has 0.4707 and 0.718 is obtained for the Friedmann-Lemaître metric. Combined with the size of FBGs, it is clear that $D_L \neq D_A(1+z)^2$.

The fourth cosmological test allows the time-dependence of various models to be compared. Close pair fractions for disks (Kartaltepe et al. 2007) [22] are applied to a $<2.88\ Gyr>$ merger time with respect to simulations (Lotz et al. 2008) [28]. This merger time is somewhat fiducial in favor of ΛCDM, as the merger process occurs at a faster rate due to the inclusion of dark matter. The simulated galaxies are similar to the FBGs applied in the angular scale test, undergoing a major merger once on average by $1.355z$ (Lotz et al. 2011) [29]. Time dependence of each model is therefore applied to determine the merger time required to reach one major merger by $1.355z$. With respect to the steady state, the relative age of distant galaxies increases with redshift. The local remnant fraction must be included in the final amount, which is much less than 3% with respect to the New General Catalog. The steady state with local expansion requires a merger time of $<3.70\ Gyr>$ and $<3.72\ Gyr>$ without. ΛCDM and Friedmann-Lemaître provide $<0.491\ Gyr>$ and $<0.332\ Gyr>$ respectively.

The final test applies several of the previous constraints in order to determine the amount of FBGs with respect to each model. These allow number density and the redshift distribution of FBGs to be compared between 20B and 23B. These magnitudes correspond to galaxies prior to $0.7z$ as confirmed by spectroscopic redshift surveys. It is known from observations that minimal evolution occurs with respect to the bulk of these objects. For example, only 8.3% of the imaged FBGs were close pairs with even fewer remnants. On time-scales predicted by the steady state with $<2.88\ Gyr>$ merger times, the amount of galaxies decreases by 15.0% for $0.5z$.

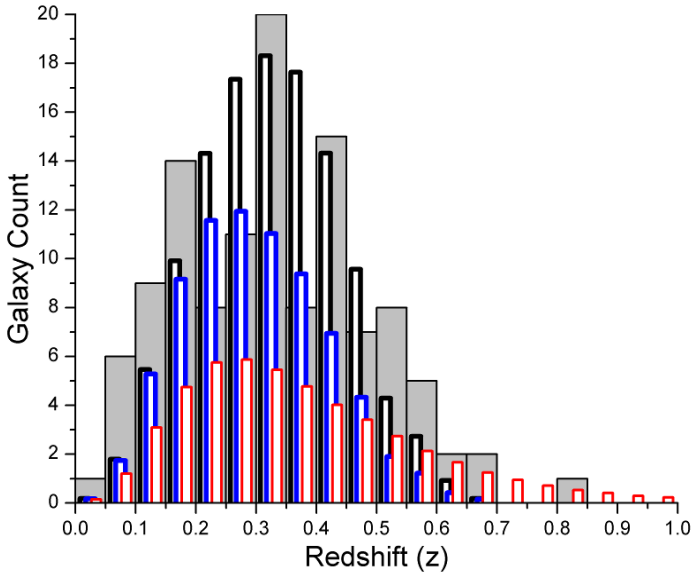

Figure 4. Predicted versus observed FBG counts between 20B and 23B, mergers and UV corrections were included.

Table 2. Color and UV properties of common disk galaxies

Color	**Sa/ab**	**Sb/bc**	**Sc/cd**	**Sd**	**Im**
(B - I)	2.04	1.96	1.55	1.34	1.19
(B - R)	1.42	1.35	1.08	0.952	0.845
(4250A − 3320A)	-0.890	-0.642	-0.556	-0.420	-0.210
(4250A − 2980A)	-1.30	-0.918	-0.844	-0.440	-0.345
(4250A − 2460A)	-1.94	-1.58	-1.04	-0.447	-0.213
(4250A − 1910A)	-1.87	-1.60	-0.663	-0.177	0.248

Redshift surveys from Colless et al. (1989) [6] and Glazebrook et al. (1995) [12] are compared to the predictions of each model in figure **4**. The local references were applied with merger fractions and <2.88 Gyr> merger times. Colless et al. (1989) [6] concluded that at least half of the ΛCDM abundance occurs prior to $0.5z$. The steady state without evolution predicts $2.10x$ the amount of galaxies with respect to ΛCDM between $0.2z$ and $0.6z$. After applying UV corrections and mergers, this decreased to $1.69x$. The steady state however still has nearly twice the amount of galaxy counts between $0.35z$ and $0.65z$ as depicted by figure **4**. Prior to 0.2z the steady state and ΛCDM provide similar predictions, indicating an insufficient FBG dataset or that local galaxies in figure **2** do not represent the entire FBG population. Many counts between $0.2z$ and $0.4z$ however are much lower than expected with respect to the known abundance.

FBGs with high-resolution imaging consist almost entirely of late disk beyond $0.5z$. Their OII widths vary, while enhanced star formation is occurring with bluer (B - R) colors of <1.07>. Starburst galaxies fit into this category with UV colors of (4250A − 2460A) > −0.3. Starburst FBGs include 10.2.02, 10.2.04 and 13.2.26, which provide $(b_j - r_F)$ colors of 0.73, 0.58 and 0.64 respectively (Colless et al. 1994) [7]. The mean redshift of these FBGs is $0.56z$, demonstrating that the bulk of galaxies beyond $0.5z$ are very blue and bright. OII widths were relatively low indicating starburst galaxies rather than AGN.

4 Discussion

Redshift versus distance modulus of SNIa allows two of the four models to be ruled out, i.e. only the steady state with residual thermal expansion and ΛCDM agree with observations. Beyond the standard deviation relative to SNIa, these models are differentiated by predictions of directional dependence and bulk flow. Bulk flow and directional dependence of SNIa has been observed (Turnbull et al. 2012) [48]. A bulk flow of clusters known as the "dark flow" is also detected within WMAP (Kashlinsky et al. 2010) [24] and PLANCK (Atrio-Barandela 2013) [1] datasets. These observations are therefore consistent with the steady state model rather than ΛCDM.

Predictions of angular diameter distances offer a more conclusive differentiation between models. FBG size versus magnitude favors the steady state, where disagreement with ΛCDM increases with redshift. Variations in galaxy and cluster angular sizes are also nearly equivalent up to $0.7z$. Higher redshift galaxies in the HUDF are $10x$ smaller than the FBG populations, with many only undergoing a single major merger. Curvature however is a minor component with respect to the effects of metric expansion in big bang cosmology. This expansion is the main factor in angular diameter distances being too small with respect to direct observations.

Relative to the CMBR, these results provide serious consequences for big bang cosmologies. Radiation in equilibrium has an energy density related to temperature via $u = \sigma T^4$. Variations in temperature and wavelength are defined by a scale factor $T(z) = T_0/a(t)$ and cosmological redshift $\lambda\,(z) = \lambda_0/(1+z)$. However, the scale factor is not equal to $(1+z)^{-1}$ as demonstrated by various tests. Temperature and wavelength will therefore vary disproportionately, failing to preserve the observed black body spectrum. The boson interpretation of the CMBR is therefore ruled out. This further invalidates recent WMAP (Jarosik et al. 2011) [21] and prior curvature results due to flawed assumption. The more constrained measurements of clusters and galaxies depict a steady-state projection with negative curvature.

The properties of clusters and galaxies over various redshift provide additional insight into these observations. Time-scales between models are drastically different, where the steady state has nearly 600% and 750% additional proper time between $0z$ and $1z$ relative to ΛCDM and the Friedmann-Lemaître model respectively. The fourth test demonstrated that time scales are in agreement with the steady state. This model also requires for distant galaxies and clusters to be older than local populations. In this perspective, galaxies and clusters are expected to cool with redshift. Merger fractions and remnants are also predicted to increase with redshift, while the opposite is true for big bang cosmologies. Local clusters are abundant in x-ray emitting gas, with dimensions similar to that of distant Lyman-alpha blobs. Lyman-alpha blobs however consist of reionized hydrogen, which is the product of x-ray emitting gas that has cooled over billions of years. Observations therefore insist clusters are cooling with increased redshift.

Distant galaxies follow a trend similar to that of clusters, where cooling occurs with increased redshift. Recent observations indicate a drastic increase in cold baryonic matter up to moderate redshift. For example, fractions of cold baryonic matter increase to 34% and 44% by 1.2z and 2.3z respectively (Tacconi et al. 2010) [47]; this is 300% to 1000% more than local galaxies. The additional cold baryonic matter promotes star formation beyond 0.5z (Guillemin et al. 1997) [15] with higher rates beyond 1.5z (Connolly et al. 1997) [8]. These observations are reinforced by the local abundance of Mg, which is higher in early type galaxies. Elliptical and lenticular galaxies are abundant in stars that will undergo type

Table 3. Results of cosmological tests (lower is better)

Test	Steady State With Expansion	Steady State Without Expansion	ΛCDM	Friedmann-Lemaître
1	0.5305	2.1647	0.5381	1.1969
2	8.836	8.840	15.01	11.12
3	0.2192	0.2054	0.4707	0.7180
4	28.5%	29.2%	83.0%	88.5%
5	4.12	4.17	4.34	6.15
Score	**1.206**	**4.786**	**13.70**	**52.01**

II supernova, which produce the majority of local Mg. Weak MgII absorbers are instead abundant at moderate redshift to 2.2z (Steidel et al. 1992) [44]. This is in agreement with the relatively high FeII:MgII ratios in distant quasars (Maiolino et al. 2003) [30], i.e. galactic metallicity is increasing with redshift. Observations are therefore fully consistent with the proper age of galaxies and clusters increasing with redshift.

The fraction of merger remnants and redshift dependence of close merger pairs demonstrate two important observations. Less than 0.5% of NGC galaxies can be considered major merger remnants, increasing to $> 25\%$ with red galaxies in the HUDF ($> 1.0z$). For disk galaxies, tidal tails or multiple cores are significant features of major merger remnants. Close pair fractions also significantly increase at high redshift (Bluck et al. 2009) [3] with few major mergers taking place locally. Similar observations are found for low and high redshift clusters. For example, cluster merger fractions are 0.1 to 0.5 up to moderate redshift, with a decreasing fraction of relaxed clusters starting beyond $0.4z$ (Mann et al. 2011) [31]. Observations are therefore consistent with local expansion due to prior cooling of dense x-ray emitting gas. Expansion however is temporary as indicated by increased merger remnants and merger fractions at moderate redshift.

Various observations with respect to galactic evolution imply that the bottom-up approach to formation is incorrect. Clusters and galaxies are instead consistent with the products of x-ray emitting gas cooling into "collapsing galaxies" (Eggen et al. 1962) [11]. Morphologies in massive clusters provide additional insight into active and passive galaxies. Passive galaxies in clusters commonly exist in regions abundant with x-ray emitting gas, while active galaxies exist along the outer perimeters. X-ray emitting gas inhibits the formation of stellar populations and initial collapse of galaxies. With respect to the various disk morphologies, Sa, Sab and Sb have smaller diameters when compared to Sc, Scd and Sd of equivalent absolute B-magnitude. The rotational curves of disk galaxies and increasing diameters with later types imply that galaxies evolve from early elliptical into late-type disk. The stellar populations of various morphologies also agree with the collapsing gas model, as elliptical galaxies contain abundant amounts of metal poor stars and hot gas. Disk galaxies however have increased dust, star formation rates and population I stars. It is therefore expected for the number density of elliptical galaxies to decrease at moderate and high redshift, where disk and merger remnants become abundant.

It is concluded that models based upon an expanding space-time metric are ruled out from poor predictions of angular diameter distances and time-dependence. Observations are instead consistent with an asymptotically flat, steady state model. The recently discovered bulk flow of clusters in WMAP and PLANCK data is the product of a continuous jet emanating from the center of an asymptotically flat gravitational potential. This relativistic

jet is much larger than those observed from local quasars, decaying into a dense proton, electron and neutrino gas. The dark flow consists of large regions of hot, x-ray emitting gas as measured by the Sunyaev–Zel'dovich effect (Kashlinsky et al. 2009) [23].

The CMBR is blackbody radiation emitted from the surface of a central core. The 2.73K spectrum has been shifted into the microwave region by gravitational redshift, which preserves the characteristic blackbody shape. Entropy is globally constant with the central core having properties of superfluidity and superconductivity. Matter is effectively expelled at the poles, where it later falls back into the potential at relativistic speeds. Momentum and energy are conserved, with two relativistic jets depicted by hot strips in the cleaned CMBR images.

Additional surveys and studies are necessary for improving the various tests. The sample of high-resolution FBGs and UV properties of disk galaxies must be increased. Surveys of clusters between 1 and $2z$ will also fill in the transitional gap between the local abundance of hot x-ray emitting gas and reionized hydrogen at high redshift. Merger fractions with small separation distances must be adjusted relative to proper angular diameter distances. Merger simulations should also be conducted without dark matter to remove any fiducial aspects.

References

[1] Atrio-Barandela F., *On the Statistical Significance of the Bulk Flow Measured by the PLANCK Satellite*, *A&A* (Accepted 2013) arXiv:1303.6614.

[2] Axelsson M., Fantaye Y., Hansen F. K., Banday A. J., Eriksen H. K., Gorski K. M., *Directional dependence of ΛCDM cosmological parameters*, *ApJ* **773** (2013) L3 arXiv:1303.5371.

[3] Bluck A., Conselice C., Bouwens R., Daddi E., Dickinson M., Papovich C., Yan H., *A Surprisingly High Pair Fraction for Extremely Massive Galaxies at $z \sim 3$ in the GOODS NICMOS Survey MNRAS* **394** (2009) 51 arXiv:0812.0926.

[4] Broadhurst T. J., Ellis R. S., Shanks T., *The Durham/Anglo-Australian Telescope faint galaxy redshift survey MNRAS* **235** (1988) 827.

[5] Code A., Welch H., *Ultraviolet photometry from the Orbiting Astronomical Observatory. XL - The energy distributions of spiral and irregular galaxies ApJ* **256** (1982) 1C.

[6] Colless M. M., Ellis R. S., Taylor K., Hook R. N., *The LDSS deep redshift survey MNRAS* **244** (1989) 408C.

[7] Colless M., Schade D., Broadhurst T. J., Ellis R., *High-resolution imaging of faint blue galaxies MNRAS* **267** (1994) 1108 arXiv:astro-ph/9401028.

[8] Connolly A. J., Szalay A. S., Dickinson M., SubbaRao M. U., Brunner R. J., *The Evolution of the Global Star Formation History as Measured from the Hubble Deep Field ApJ* **486** (1997) L11 arXiv:astro-ph/9706255.

[9] Dey A., Bian C., Soifer B., Brand K., Brown M., Chaffee F., LeFloc'h E., Hill G., Houck J., Jannuzi B., Rieke M., Weedman D., Brodwin M., Eisenhardt P., *Discovery of a Large ∼200 kpc Gaseous Nebula at $z = 2.7$ with the Spitzer Space Telescope ApJ* **629** (2005) 654 arXiv:astro-ph/0503632.

[10] Driver S., Couch W., Phillipps S., Windhorst R., *The Inferred Redshift Distribution of the Faint Blue Galaxy Excess ApJ* **466** (1996) L5 arXiv:astro-ph/9605048.

[11] Eggen O., Lynden-Bell D., Sandage A., *Evidence from the motions of old stars that the Galaxy collapsed ApJ* **136** (1962) 748.

[12] Glazebrook K., Ellis R., Colless M., Broadhurst T., Griffiths R., Allington-Smith J., Tanvir N., *A faint galaxy redshift survey to $B = 24$ MNRAS* **273** (1995) 157G arXiv:astro-ph/9503116.

[13] Greve T. R., Stern D., Ivison R. J., De Breuck C., Kovács A., Bertoldi F., *Wide-field mid-infrared and millimetre imaging of the high-redshift radio galaxy, 4C41.17. MNRAS* **382** (2007) 48G arXiv:0707.4482.

[14] Gronwall C., Koo D. C., *Resurrection of traditional luminosity evolution models to explain faint field galaxies ApJ* **440L** (1995) 1G arXiv:astro-ph/9411062.

[15] Guillemin P., Bergeron J., *Evolution of quasar absorption-selected galaxies A&A* **328** (1997) 499 arXiv:astro-ph/9705170.

[16] Häring N., Rix H., *On the Black Hole Mass-Bulge Mass Relation ApJ* **604** (2004) L89 arXiv:astro-ph/0402376.

[17] Hatch N. A., Overzier R. A., Kurk J. D., Miley G. K., Röttgering H. J. A., Zirm A. W., *The growth and assembly of a massive galaxy at z∼2 MNRAS* **395** (2009) 114 arXiv:0901.3353.

[18] He P., Zhang Y., *Modelling the number counts of early-type galaxies by pure luminosity evolution MNRAS* **298** (1998) 483 arXiv:astro-ph/9802118.

[19] Hubble E. P., *A relation between distance and radial velocity among extra-galactic nebulae Proc. Natl Acad. Sci.* **15** (1929) 168

[20] Ivison R. J., Smail I., Le Borgne J. F., Blain A. W. Kneib J. P., Bezencourt J., Kerr T. H., Davies J. K., *A hyperluminous galaxy at z = 2.8 found in a deep submillimetre survey MNRAS* **298** (1998) 583 arXiv:astro-ph/9712161.

[21] Jarosik N., Bennett C. L., Dunkley J., Gold B., Greason M. R., Halpern M., Hill R. S., Hinshaw G., Kogut A., Komatsu E., Larson D, Limon M., Meyer S. S., Nolta M. R., Odegard N., Page L., Smith K. M., Spergel D. N., Tucker G. S., Weiland J. L., Wollack E., Wright E., *Seven-year Wilkinson Microwave Anisotropy Probe (WMAP) Observations: Sky Maps, Systematic Errors, and Basic Results ApJS* **192** (2011) 14 arXiv:1001.4744.

[22] Kartaltepe J. S., Sanders D. B., Scoville N. Z., Calzetti D., Capak P., Koekemoer A., Mobasher B., Murayama T., Salvato M., Sasaki S., Taniguchi Y., *Evolution of the Frequency of Luminous ($\geq L_V*$) Close Galaxy Pairs at z < 1.2 in the COSMOS Field* ApJS* **172** (2007) 320 arXiv:0705.2266.

[23] Kashlinsky A., Atrio-Barandela F., Kocevski D., Ebeling H., *A measurement of large-scale peculiar velocities of clusters of galaxies: technical details ApJ* **691** (2009) 1479 arXiv:0809.3733.

[24] Kashlinsky A., Atrio-Barandela F., Ebeling H., Edge A., Kocevski D., *A new measurement of the bulk flow of X-ray luminous clusters of galaxies ApJ* **712** (2010) L81 arXiv:0910.4958.

[25] Keel W. C., Cohen S. H., Windhorst R. A., Waddington I., *Evidence for Large-Scale Structure at z ≈ 2.4 from Ly-α Imaging AJ* **118** (1999) 2547 arXiv:astro-ph/9908183.

[26] Lemaître G., *Un univers homogene de masse constante et de rayon croissant, rendant compte de la vitesse radiale des nebuleuses extra-galactiques Ann. Soc. Sci. Brux.* **A 47** (1927) 49

[27] Lemaux B. C., Lubin L. M., Shapley A., Kocevski D., Gal R. R., Squires G. K., *The origin of [O II] in post-starburst and red-sequence galaxies in high-redshift clusters ApJ* **716** (2010) 970 arXiv:1003.1780.

[28] Lotz J. M., Jonsson P., Cox T. J., Primack J. R., *Galaxy merger morphologies and time-scales from simulations of equal-mass gas-rich disc mergers MNRAS* **391** (2008) 1137 arXiv:0805.1246.

[29] Lotz J. M., Jonsson P., Cox T. J., Primack J. R., Somerville R. S., Stewart K., *The Major and Minor Galaxy Merger Rates at z < 1.5z ApJ* **742** (2011) 103 arXiv:1108.2508.

[30] Maiolino R., Juarez Y., Mujica R., Nagar N. M., Oliva E., *Early Star Formation Traced by the Highest Redshift Quasars ApJ* **596** (2003) L155 arXiv:astro-ph/0307264.

[31] Mann A. W., Ebeling H., *X-ray/optical classification of cluster mergers and the evolution of the cluster merger fraction* arXiv:1111.2396.

[32] Maughan B. J., Jones C., Forman W., Van Speybroeck L., *Images, Structural Properties, and Metal Abundances of Galaxy Clusters Observed with Chandra ACIS-I at 0.1 <z < 1.3 ApJS* **174** (2008) 117 arXiv:astro-ph/0703156.

[33] McDonald, *Baryon-to-Dark Matter Ratio from Random Angular Fields JCAP* **1301** (2013) 25 arXiv:1211.4472.

[34] Mehrtens N., Romer A., Hilton M., Lloyd-Davies E., Miller C., Stanford S., Hosmer M., Hoyle B., Collins C., Liddle A., Viana P., Nichol R., Stott J., Dubois N., Kay S., Sahlen M., Young O., Short C., Christodoulou L., Watson W., Davidson M., Harrison C., Baruah L., Smith M., Burke C., Mayers J., Deadman P., Rooney P., Edmondson E., West M., Campbell H., Edge A., Mann R., Sabirli K., Wake D., Benoist C., da Costa L., Maia M., Ogando R., *XCS-DR1 Cluster Catalogue MNRAS* **423** (2012) 1024

[35] **NED, 2013.** This research has made use of the NASA/IPAC Extra-galactic Database (NED) which is operated by the Jet Propulsion Laboratory, California Institute of Technology, under contract with the National Aeronautics and Space Administration

[36] Nilson P., *Uppsala General Catalogue of Galaxies (UGC) Uppsala Astron. Obs. Ann.* **6** (1973)

[37] Nilsson K. K., Fynbo J. P. U., Møller P., Sommer-Larsen J., Ledoux C., *A Lyman-α blob in the GOODS South field: evidence for cold accretion onto a dark matter halo A&A* **452** (2006) L23 arXiv:astro-ph/0512396.

[38] Ouchi M., Ono Y., Egami E., Saito T., Oguri M., McCarthy P. J., Farrah D., Kashikawa N., Momcheva I., Shimasaku K., Nakanishi K., Furusawa H., Akiyama M., Dunlop J. S., Mortier A. M. J., Okamura S., Hayashi M., Cirasuolo M., Dressler A., Iye M., Jarvis M. J., Kodama T., Martin C. L., McLure R. J., Ohta K., Yamada T., Yoshida M., *Discovery of a Giant Lyα Emitter Near the Reionization Epoch ApJ* **696** (2009) 1164 arXiv:0807.4174.

[39] Peck M. S., *The Theory of Everything: Foundations, Applications and Corrections to General Relativity* viXra:1305.0138.

[40] Roche P., Coe M. J., Fabregat J., McHardy I. M., Norton A. J., Percy J. R., Reglero V., Reynolds A., Unger S. J., *Angular sizes of the faint blue galaxies MNRAS* **288** (1997) 200

[41] Roettiger K., Stone J. M., Burns J. O., *Magnetic Field Evolution in Merging Clusters of Galaxies ApJ* **518** (1999) 594 arXiv:astro-ph/9902105.

[42] Saito T., Shimasaku K., Okamura S., Ouchi M., Akiyama M., Yoshida M., Ueda Y., *Deep Spectroscopy of Systematically Surveyed Extended Lyα Sources at z = 3-5 ApJ* **675** (2008) 1076 arXiv:0705.1494.

[43] Smith D. J. B., Jarvis M. J., Lacy M. Martinez-Sansigre A., *Infrared and millimetre-wavelength evidence for cold accretion within a z= 2.83 Lyman-α blob MNRAS* **389** (2008) 799 arXiv:0806.4384.

[44] Steidel C. C., Sargent W. L. W., *MG II absorption in the spectra of 103 QSOs-Implications for the evolution of gas in high-redshift galaxies ApJS* **80** (1992) 1

[45] Steidel C. S., Adelberger K. L., Shapley A. E., Pettini M., Dickinson M., Giavalisco M., *Lyα Imaging of a Proto-Cluster Region at <z> = 3.09 ApJ* **532** (2000) 170 arXiv:astro-ph/9910144.

[46] Stutz A., Papovich C., Eisenstein D., *On the Stellar Populations in Faint Red Galaxies in the Hubble Ultra Deep Field ApJ* **677** (2008) 828 arXiv:0801.2388.

[47] Tacconi L. J., Genzel R., Neri R., Cox P., Cooper M. C., Shapiro K., Bolatto A., Bouché N., Bournaud F., Burkert A., Combes F., Comerford J., Davis M., Förster Schreiber N. M., Garcia-Burillo S., Gracia-Carpio J., Lutz D., Naab T., Omont A., Shapley A., Sternberg A.,

Weiner B., *High molecular gas fractions in normal massive star-forming galaxies in the young Universe Nature* **463** (2010) 781 arXiv:1002.2149.

[48] Turnbull S. J., Hudson M. J., Feldman H. A., Hicken M., Kirshner R. P., Watkins R., *Cosmic flows in the nearby universe from Type Ia supernovae MNRAS* **420** (2012) 447 arXiv:1111.0631.

[49] de Vaucouleurs G., de Vaucouleurs A., Corwin Jr. H. G., Buta R. J., Paturel G., Fouque P., *Third Reference Catalogue of Bright Galaxies* 1991,

[50] Venemans B., Kurk J., Miley G., Röttgering H., van Breugel W., Carilli C., De Breuck C., Ford H., Heckman T., McCarthy P., Pentericci L., *The Most Distant Structure of Galaxies Known: A Protocluster at z = 4.1 ApJ* **569** (2002) L11 arXiv:astro-ph/0203249.

[51] Wei H.,*Observational Constraints on Cosmological Models with the Updated Long Gamma-Ray Bursts JCAP* **1008** (2010) 20 arXiv:1004.4951.

[52] Williamson R., Benson B. A., High F. W., Vanderlinde K., Ade R. P. A., Aird K. A., Andersson K., Armstrong R., Ashby M. L. N., Bautz M., Bazin G., Bertin E., Bleem L. E., Bonamente M., Brodwin M., Carlstrom J. E., Chang C. L., Chapman S. C., Clocchiatti A., Crawford T. M., A. T. Crites, de Haan T., Desai S., Dobbs M. A., Dudley J. P., Fazio G. G., Foley R. J., Forman W. R., Garmire G., George E. M., Gladders M. D., Gonzalez A. H., N. W. Halverson, Holder G. P., Holzapfel W. L, Hoover1 S., Hrubes J. D., Jones C., Joy M., Keisler R., Knox L., Lee A. T., Leitch E. M., Lueker M., Luong-Van D., Marrone1 D. P., McMahon J. J., Mehl J., Meyer S. S., Mohr J. J., Montroy T. E., Murray S. S., Padin S., Plagge T., Pryke1 C., Reichardt C. L., Rest A., Ruel J., Ruhl J. E., Saliwanchik B. R., Saro A., Schaffer K. K., Shaw L., Shirokoff E., Song J., Spieler H. G., Stalder B., Stanford S. A., Staniszewski Z., Stark A. A., Story K., Stubbs C. W., Vieira J. D., Vikhlinin A., Zenteno A., *A Sunyaev-Zel'dovich selected Sample of the Most Massive Galaxy Clusters in the 2500 deg^2 South Pole Telescope Survey ApJ* **738** (2011) 139 arXiv:1101.1290.

[53] Willott C. J., Chet S., Bergeron J., Hutchings J. B., *A Lyα Halo around a Quasar at Redshift z = 6.4 AJ* **142** (2011) 186 arXiv:1109.4110.